Visible-Light-Driven Tunable Molecular Motors Based on Oxindole

Roke, Diederik; Sen, Metin; Danowski, Wojciech; Wezenberg, Sander J.; Feringa, Ben L.

Published in:
Journal of the American Chemical Society

DOI:
10.1021/jacs.9b03237

Publication date:
2019

JACS JOURNAL OF THE AMERICAN CHEMICAL SOCIETY

Article

Cite This: J. Am. Chem. Soc. 2019, 141, 7622−7627

pubs.acs.org/JACS

Visible-Light-Driven Tunable Molecular Motors Based on Oxindole

Diederik Roke, Metin Sen, Wojciech Danowski, Sander J. Wezenberg,*,† and Ben L. Feringa*

Stratingh Institute for Chemistry, University of Groningen, Nijenborgh 4, 9747 AG, Groningen, The Netherlands

Supporting Information

ABSTRACT: Molecular rotary motors based on oxindole which can be driven by visible light are presented. This novel class of motors can be easily synthesized via a Knoevenagel condensation, and the choice of different upper halves allows for the facile tuning of their rotational speed. The four-step rotational cycle was explored using DFT calculations, and the expected photochemical and thermal isomerization behavior was confirmed by NMR, UV/vis, and CD spectroscopy. These oxindole motors offer attractive prospects for functional materials responsive to light.

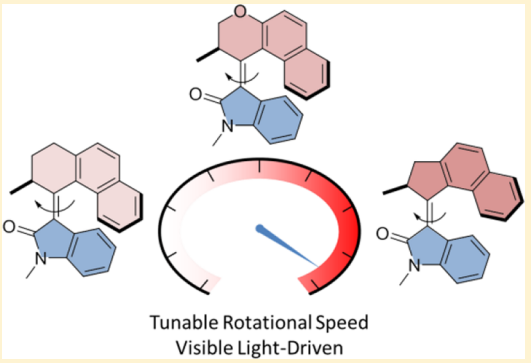

INTRODUCTION

The emergence of artificial molecular machines has allowed the chemist to control motion at the nanoscale.[1−7] Among these machines, molecular rotary motors are particularly attractive, owing to their unique ability to undergo repetitive unidirectional rotation and to drive systems out of equilibrium.[8−10] Overcrowded alkene-based motors, which are driven by light, have shown great potential in a number of fields, such as soft materials,[11−14] catalysis,[15] and surface chemistry,[16] enabling responsive and dynamic behavior. They were first reported by our group in 1999,[17] and since then, second and third generation molecular motors have been developed and their functioning has been thoroughly investigated.[18,19] Through synthetic modification, the rotational speed can be tuned,[8,20,21] and recently, alternative methods to dynamically control their rotary motion have been developed.[22−24] A major challenge that remains, for molecular motors to reach their full potential,[9,10] is to drive the rotation with visible light instead of harmful UV light.[25] Strategies to shift the excitation wavelength to the visible range have been developed by, for example, making use of photosensitizers,[22,26] extended π systems,[27] or push−pull substituents.[28] Apart from adapting the design of existing motors, new types of light-driven molecular motors are highly warranted. Lehn and co-workers reported easily accessible molecular motors based on imines,[29,30] and the group of Dube developed molecular motors based on hemithioindigo.[31−33] Here we present molecular motors that are based on arylidene oxindoles, which are easily accessible by a condensation reaction and can be operated by visible light.

The group of Luňák showed that some arylidene oxindoles undergo $E-Z$ isomerization when exposed to sunlight, but the potential of these compounds as photoswitches has, to the best of our knowledge, not yet been explored.[34] Inspired by the facile synthesis and the interesting spectroscopic properties of arylidene oxindoles, we envisioned a new design for a molecular rotary motor.

Our design features an *N*-methyloxindole lower half and an upper half similar to molecular motors based on overcrowded alkenes[17−19] connected through a central double bond functioning as a rotary axle (Scheme 1a). Molecular motors **1**−**4** can be readily synthesized, and the oxindole scaffold provides an attractive handle for further functionalization. For distinct application, often a specific rotational speed is required.[9,10] Therefore, structures with five- and six-membered rings (X = CH_2, O, and S) were chosen, in analogy to other molecular motors based on overcrowded alkenes, as they have been shown to have large differences in rotational speed.[34,35] These upper halves all bear a methyl stereocenter that dictates the direction of rotation. A rotation cycle much like molecular motors based on overcrowded alkenes is proposed,[17−19] with the first step being a photochemical $E-Z$ isomerization (PEZ) converting stable *E*-**1** to unstable *Z*-**1** (Scheme 1b). In this isomer, the methyl at the stereocenter adopts an unfavorable (pseudo)axial orientation. To release some of the strain, both halves can slip along each other in a thermal helix inversion (THI), forming stable *Z*-**1** and completing the first half of the rotary cycle. In a similar fashion, a second photochemical isomerization followed by a THI takes place to complete a 360° rotation. Key to the unidirectional rotation is that upon photochemical $E-Z$ isomerization, an unstable state is formed that undergoes an energetically downhill THI process, in a forward direction being more favorable than a backward $Z-E$ isomerization.

Received: March 25, 2019
Published: April 19, 2019

DOI: 10.1021/jacs.9b03237
J. Am. Chem. Soc. 2019, 141, 7622−7627

Scheme 1. (a) Oxindole-Based Molecular Motors and (b) Representative Rotational Cycle of Motor 1

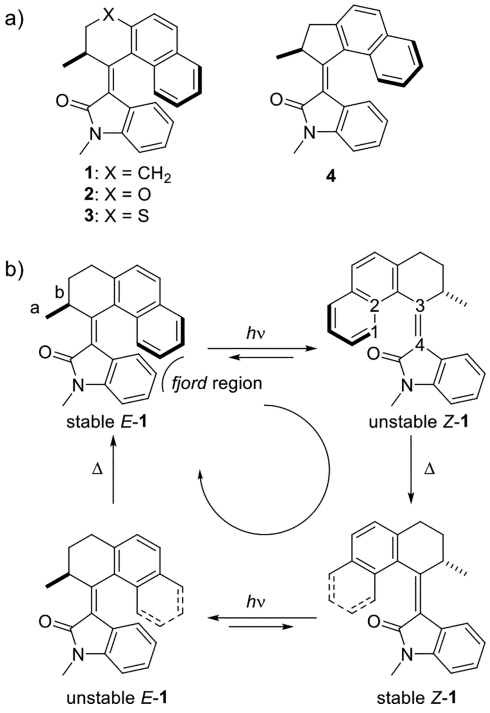

RESULTS AND DISCUSSION

Initially, DFT calculations were performed to predict the structural parameters and the relative energies of the different isomers of oxindole-based motors **1**–**4** (Figure 1). All structures were optimized using the B3LYP functional with a 6-31+G(d,p) basis set. Additionally, a IEFPCM, DMSO solvation model was chosen as previous studies with arylidene oxindoles were carried out in DMSO.[34] The calculated relative Gibbs free energies of all stable and unstable states as well as the transition states (TS) for THI are shown in Figure 1. In all cases, two unstable states are found that are much higher in energy than their respective stable states with opposite helicity. This energy difference is crucial to ensure unidirectionality in the rotary cycle of molecular motors. The relative energy barriers for THI of all motors are summarized in Table 1.

Table 1. DFT Calculated Barriers for THI of 1–4

	$\Delta^{\ddagger}G^{calc}$ (*Z*) (kJ mol^{-1})	$\Delta^{\ddagger}G^{calc}$ (*E*) (kJ mol^{-1})	dihedral angle[a] (deg)
1	98.8	110.3	43.1
2	87.6	100.4	41.2
3	108.5	120.2	48.1
4	53.3	66.8	23.9

[a]Dihedral angle 1–2–3–4 in unstable-*Z* as shown in Scheme 1b.

Similar to what has been reported for their overcrowded alkene-based counterparts,[35−37] motors **1**–**3** with a central six-membered ring in the upper half have higher barriers than motor **4** with a five-membered ring. The latter has less steric hindrance in the fjord region, making it easier for the two halves to slide along each other. In all cases, the barrier for THI of unstable-*Z* is lower than for unstable-*E* which can also be explained by less steric hindrance in the fjord region as here the upper half needs to pass the smaller carbonyl instead of the bulkier aromatic ring. Furthermore, the calculated barriers for THI in motors **1**–**3** scale with the size of the bridging atom X (S > C > O). The upper half is pushed closer toward the lower half as the size of X increases, causing more steric hindrance in the fjord region. As a consequence, the upper half folds away from the lower half, resulting in an increased dihedral angle 1–2–3–4 in unstable-*Z* (Table 1). A similar effect has been observed in overcrowded alkene-based molecular motors.[36] The results of these calculations indicate that oxindole-based molecular motors **1**–**4** will operate as unidirectional rotary molecular motors.

Oxindole motors **1**–**4** were synthesized in a single step by a Knoevenagel condensation of commercially available *N*-methyloxindole and the corresponding ketone, mediated by a combination of $TiCl_4$ and DBU (Scheme 2). The ketones were

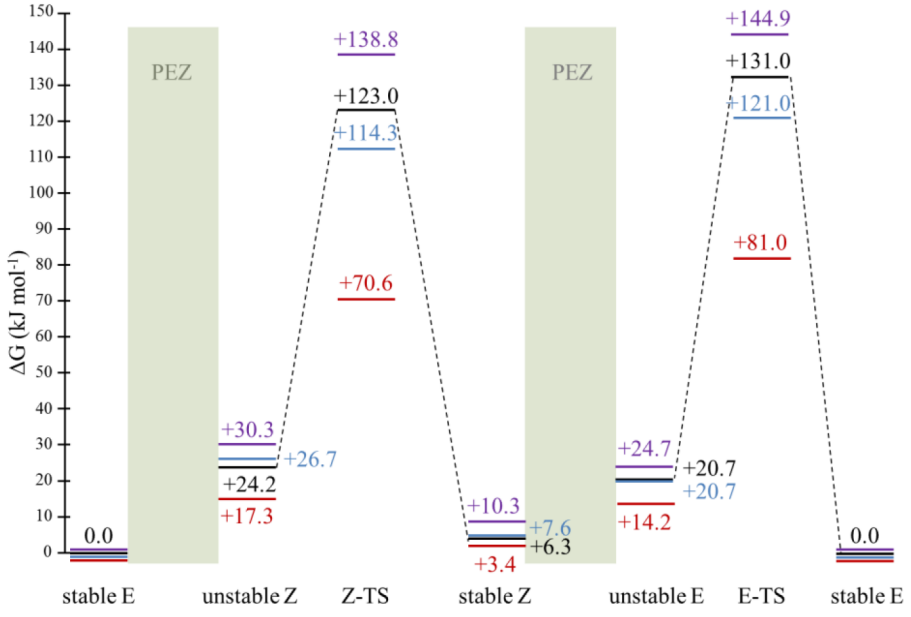

Figure 1. Calculated relative Gibbs free energies of motors **1** (black), **2** (blue), **3** (purple), and **4** (red).

DOI: 10.1021/jacs.9b03237
J. Am. Chem. Soc. 2019, 141, 7622−7627

Scheme 2. Representative Synthesis of Molecular Motor 1 and Isolated Yields of 1−4

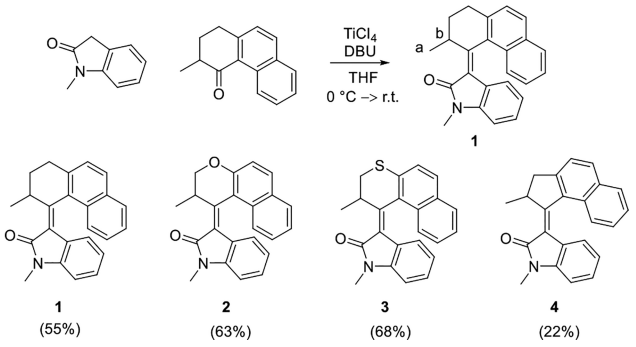

synthesized in one to four steps following well-established literature procedures,[36,38] thus making these molecular motors very easily accessible. In all cases the *E*-isomer was exclusively obtained. According to DFT calculations, this isomer is the most stable one (vide infra).

With these four different motors in hand, the photochemical and thermal isomerization behavior was first monitored by ^{1}H NMR spectroscopy with λ_{max}= 365 nm light. Upon irradiation of an NMR sample of *E*-**1** in DMSO-d_6 at room temperature, a new set of signals appeared (Figures 2 and S2).[39] The most distinct shifts were observed for protons H_a (1.02 → 1.39) and H_b (4.85 → 4.02) at the stereogenic center (see Scheme 1 for the atom labeling). Hence, these ^{1}H NMR spectral changes were ascribed to formation of the unstable *Z*-isomer. The sample was irradiated until no further changes were observed, and at this photostationary state (PSS) the ratio of unstable *Z*-**1** to stable *E*-**1** was 76:24. Heating this sample to 60 °C resulted in the disappearance of the signals assigned to this photogenerated isomer. A new stable state was obtained, and isolation and characterization of the newly obtained isomer on preparative scale revealed it to be the stable *Z*-isomer. This confirms that the oxindole-based motor undergoes an *E*−*Z* isomerization upon irradiation which, followed by a THI to complete 180° rotation, is identical to other molecular motors based on overcrowded alkenes.[17] When the NMR sample containing stable *Z*-**1** was once again irradiated with λ_{max} = 365 nm light, a new set of signals appeared indicative of unstable *E*-**1**, with a PSS_{365} ratio of 96:4. Upon heating to 100 °C, the unstable isomer was converted to the original isomer (stable *E*-**2**), and as a consequence, a 360° rotation was successfully achieved. The cycle was repeated using λ_{max}= 420 nm light (Figure S3), showing that rotary motion can also be achieved with visible light.

A similar rotational cycle was observed for motor **2** in THF-d_8 (Figure S5). THF was chosen as low temperature studies were needed. Irradiation of a sample of **2** with λ_{max} = 365 nm light at −25 °C revealed the emergence of unstable *Z*-**2** (PSS_{365} = 77:23), which underwent THI to stable *Z*-**2** when the sample was allowed to warm to room temperature. Subsequent irradiation afforded unstable *E*-**2** (PSS_{365} > 99:1), which converted to the original isomer (stable *E*-**2**) when the sample was heated to 55 °C. Similar results were obtained when the rotary cycle was performed using λ_{max} = 455 nm light (Figure S6).

For motor **3**, for which the highest barriers for THI were calculated (vide infra), the first part of the cycle was found to be identical to that of motors **1** and **2** (Figure S7). Irradiation of an NMR sample of **3** in DMSO-d_6 with λ_{max} = 365 nm light at room temperature (PSS_{365} = 79:21) and subsequent heating to 100 °C showed the formation of stable *Z*-**3**. The sample was again irradiated to show the appearance of unstable *E*-**3** (PSS_{365} = 95:5); however, when it was heated, degradation was observed. Most likely, degradation is due to the high temperature required to trigger THI, owing to the high isomerization barrier for this compound ($\Delta^{\ddagger}G^{calc}$ = 120.2 kJ mol^{-1}).

Due to the low barrier for THI, unstable *Z*-**4** could only be observed when irradiated at −90 °C (Figure S8), which was performed in CD_2Cl_2. Even at this low temperature, unstable *Z*-**4** was observed to already undergo slow THI to form stable

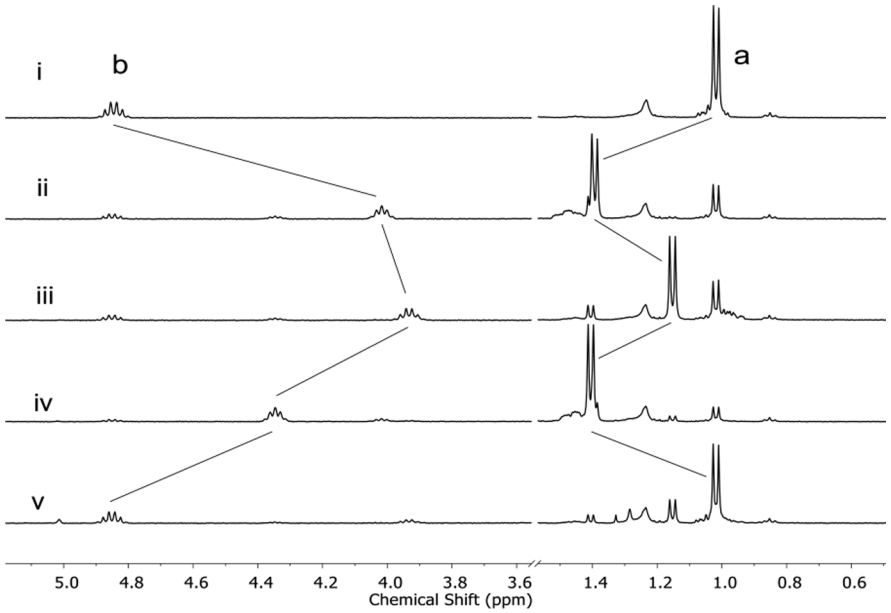

Figure 2. Selected parts of the ^{1}H NMR spectra of a sample of **1** in DMSO-d_6 (c = 2.2 × 10^{-3} M). See Scheme 1 for the atom labeling. (i) *E*-**1** before irradiation. (ii) PSS 365 nm. (iii) 60 °C, 1 h. (iv) PSS 365 nm. (v) 100 °C, 120 min.

DOI: 10.1021/jacs.9b03237
J. Am. Chem. Soc. 2019, 141, 7622−7627

Z-**4**. At the same time, this isomer then undergoes a photochemical *E*−*Z* isomerization, forming unstable *E*-**4** over time. When warming this sample to −45 °C, stable *E*-**4** is again reformed, completing 360° rotation.

Next, the photochemical and thermal isomerization behavior of motors **1**−**4** was studied using UV/vis spectroscopy. They all show a broad absorption band with λ_{max} between 350 and 400 nm, which extends into the visible region (Figure 3). Very

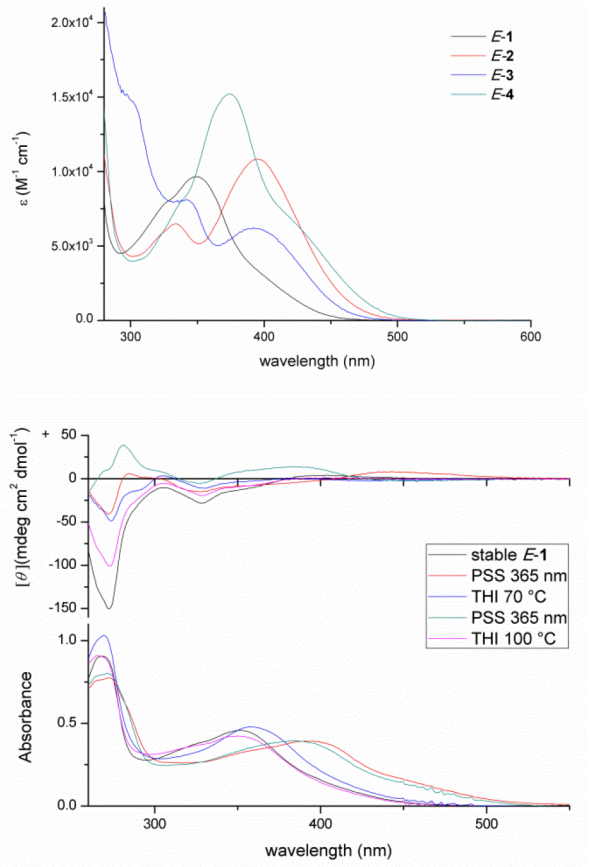

Figure 3. UV/vis spectra of motors **1**−**4** in CH_2Cl_2 (top); CD and UV/vis spectra of the rotary cycle of motor (*S*)-**1** in DMSO (bottom).

little solvatochromism (≤5 nm) was observed over a range of different solvents, including aromatic and protic solvents (Figure S12). The rotational cycle of motor **1** was additionally studied using CD spectroscopy. Its enantiomers were separated using chiral supercritical fluid chromatography and could be identified by comparing their CD spectrum to the DFT calculated spectrum (Figure S10). When a UV/vis sample of stable *E*-(*S*)-**1** in DMSO was irradiated with λ_{max} = 365 nm light, a bathochromic shift in both the UV and CD spectra could be observed, signifying the formation of unstable *Z*-(*S*)-**1** (Figure 3). Interestingly, isomerization could also be achieved with visible light of wavelengths up to 455 nm, albeit with a lower PSS, which is most likely due to the stronger absorption of the unstable isomer at longer wavelengths. Heating the sample to 60 °C leads to a blue shift of the absorption band as unstable-*Z* is converted to stable-*Z*. The helicity is inverted in this step, and as a result the sign of the CD absorption belonging to the $\pi-\pi^*$ band is changed. Subsequent irradiation of this sample with λ_{max} = 365 nm light yields the unstable *E*-isomer, which is again accompanied by a characteristic bathochromic shift, similar to that observed for the *Z*-isomer. The unstable *E*-isomer has the opposite CD sign as the starting stable *E*-isomer, as a result of their opposite helicity. Heating the sample to 100 °C completes the cycle; i.e. stable *E* is formed, which is accompanied by a hypsochromic shift.

UV/vis studies of motor **2** showed the same spectral changes as for motor **1**, with a bathochromic shift upon irradiation of the stable *E* isomer (Figure S14). In this case, isomerization was observed upon irradiation with wavelengths up to λ_{max} = 505 nm, well into the visible region. Characterization of the isomerization behavior of motor **4** with UV/vis is more challenging due to its fast THI steps. Nonetheless, a bathochromic shift could be observed upon irradiation with wavelengths up to λ_{max} = 455 nm at −30 °C, most likely originating from the unstable *E* isomer (Figure S15). The unstable *Z* isomer undergoes THI which is too fast to follow at −30 °C (note that the calculated half-life at −30 °C is 38 ms).

Eyring analysis was performed to determine the activation parameters of the THIs of motors **1**, **2**, and **4**. For compounds **1** and **2** the rate of THI was determined by following the change in absorbance at λ = 470 nm (see Figure S16 in the Supporting Information for details). For motor **4**, low temperature ^{1}H NMR was used to follow the conversion of the unstable state to the stable state (see Figure S21 in the Supporting Information for details). In each case, the rate of THI was determined at five temperatures, after which the activation parameters were obtained by using the Eyring equation (Table 2, Figures S16−S20). Due to its high rate, the

Table 2. Gibbs Free Energy Barriers of THI and Half-Lives of the Respective Unstable States of Motors 2−4[a]

	$\Delta^{\ddagger}G$ (*Z*) (kJ mol^{-1})	$t_{1/2}$	$\Delta^{\ddagger}G$ (*E*) (kJ mol^{-1})	$t_{1/2}$
1	102.2 ± 0.3	50 ± 7 h	111.7 ± 0.5	105 ± 21 d
2	87.6 ± 0.1	455 ± 14 s	101.3 ± 0.3	35 ± 5 h
4	53.5[b]		69.8 ± 1.1	305 ± 148 ms

[a]All values of $\Delta^{\ddagger}G$ and $t_{1/2}$ are at 20 °C unless otherwise noted. [b]Value determined at −94 °C.

THI of unstable *Z*-**4** to stable *Z*-**4** was followed at only one temperature (−94 °C). The Gibbs free energy barriers and half-lives of the respective unstable states are summarized in Table 2. All experimentally obtained barriers match those predicted by DFT, within a reasonable margin (≤3.4 kJ mol^{-1}). As predicted, the barriers for THI of the unstable *Z* isomers are lower for both motors **1** and **2**, and as a result, the THI of unstable *E* is the rate limiting step in the rotational cycle. These results show that half-lives ranging from milliseconds to days can be readily achieved by choosing the appropriate upper half.

Additionally, quantum yields of the photochemical isomerization steps ($\Phi_{s\rightarrow u}$) were established for motors **1** and **2** (Table 3). The rate of formation of the unstable states was

Table 3. Quantum Yields (%) of Photochemical Isomerization Steps

	Φ (%)			
	stable *E* → unstable *Z*	unstable *Z* → stable *E*	stable *Z* → unstable *E*	unstable *E* → stable *Z*
1	2.3	0.67	2.1	0.32
2	1.2	0.35	3.0	0.18

DOI: 10.1021/jacs.9b03237
J. Am. Chem. Soc. 2019, 141, 7622−7627

determined by following the absorption increase at λ = 475 nm upon irradiation of a sample with a high enough concentration to absorb all incident light. To assess the efficiency of these motors with visible light, λ_{max} = 420 nm irradiation was used. The rates thus obtained were then compared to the rate of formation of Fe^{2+} from potassium ferrioxalate under identical condition to estimate the quantum yields (Table 3; see Figures S22–S26 for details). The quantum yield for the reverse photochemical isomerization ($\Phi_{u\rightarrow s}$) could then be calculated using the PSS_{420} ratio and extinction coefficients (Table S1) at this wavelength.

CONCLUSION

In summary, readily accessible molecular motors based on oxindole have been presented that can be driven by visible light. A four-step rotation cycle was proposed based on DFT calculations and confirmed by a combination of NMR, UV/vis, and CD spectroscopy. Motors with four different upper halves were easily synthesized by a Knoevenagel condensation, allowing tuning of the half-life for THI and the overall motor speed from the millisecond regime to multiple days. Additionally, the oxindole scaffold provides a versatile handle for further functionalization, opening up new possibilities for application in biology and materials science.

ASSOCIATED CONTENT

Supporting Information

The Supporting Information is available free of charge on the ACS Publications website at DOI: 10.1021/jacs.9b03237.

Computational details, synthetic procedures and characterization, additional NMR and UV/vis spectra of the rotation cycles, Eyring plots, and details on quantum yield determination (PDF)

AUTHOR INFORMATION

Corresponding Authors

*s.j.wezenberg@lic.leidenuniv.nl
*b.l.feringa@rug.nl

ORCID

Sander J. Wezenberg: 0000-0001-9192-3393
Ben L. Feringa: 0000-0003-0588-8435

Present Address

†Leiden Institute of Chemistry, Leiden University, Einsteinweg 55, 2333 CC Leiden, The Netherlands.

Notes

The authors declare no competing financial interest.

ACKNOWLEDGMENTS

Financial support from the Ministry of Education, Culture and Science (Gravitation Program 024.001.035) and European Research Council (Advanced Investigator Grant No. 694345 to B.L.F. and Starting Grant No. 802830 to S.J.W.) is gratefully acknowledged. We thank the Center for Information Technology of the University of Groningen for their support and for providing access to the Peregrine high performance computing cluster.

REFERENCES

(1) Balzani, V.; Credi, A.; Raymo, F. M.; Stoddart, J. F. Artificial Molecular Machines. *Angew. Chem., Int. Ed.* **2000**, *39*, 3348–3391.

(2) Kinbara, K.; Aida, T. Toward Intelligent Molecular Machines: Directed Motions of Biological and Artificial Molecules and Assemblies. *Chem. Rev.* **2005**, *105*, 1377–1400.

(3) Browne, W. R.; Feringa, B. L. Making molecular machines work. *Nat. Nanotechnol.* **2006**, *1*, 25–35.

(4) Kay, E. R.; Leigh, D. A. Rise of the Molecular Machines. *Angew. Chem., Int. Ed.* **2015**, *54*, 10080–10088.

(5) Balzani, V.; Credi, A.; Venturi, M. *Molecular Devices and Machines: Concepts and Perspectives for the Nanoworld*, 2nd ed.; Wiley-VCH: Weinheim, Germany, 2008.

(6) *From Non-Covalent Assemblies to Molecular Machines*; Sauvage, J. P., Gaspard, P., Eds.; Wiley-VCH: Weinheim, Germany, 2010.

(7) Bruns, C. J.; Stoddart, J. F. *The Nature of the Mechanical Bond: From Molecules to Machines*; John Wiley & Sons, Inc.: Hoboken, NJ, 2016.

(8) Kassem, S.; van Leeuwen, T.; Lubbe, A. S.; Wilson, M. R.; Feringa, B. L.; Leigh, D. A. Artificial molecular motors. *Chem. Soc. Rev.* **2017**, *46*, 2592–2621.

(9) Roke, D.; Wezenberg, S. J.; Feringa, B. L. Molecular rotary motors: Unidirectional motion around double bonds. *Proc. Natl. Acad. Sci. U. S. A.* **2018**, *115*, 9423–9431.

(10) van Leeuwen, T.; Lubbe, A. S.; Štacko, P.; Wezenberg, S. J.; Feringa, B. L. Dynamic control of function by light-driven molecular motors. *Nat. Rev. Chem.* **2017**, *1*, 0096.

(11) Chen, J.; Leung, F. K.-C.; Stuart, M. C. A.; Kajitani, T.; Fukushima, T.; van der Giessen, E.; Feringa, B. L. Artificial muscle-like function from hierarchical supramolecular assembly of photoresponsive molecular motors. *Nat. Chem.* **2018**, *10*, 132–138.

(12) Li, Q.; Fuks, G.; Moulin, E.; Maaloum, M.; Rawiso, M.; Kulic, I.; Foy, J. T.; Giuseppone, N. Macroscopic contraction of a gel induced by the integrated motion of light-driven molecular motors. *Nat. Nanotechnol.* **2015**, *10*, 161–165.

(13) Foy, J. T.; Li, Q.; Goujon, A.; Colard-Itté, J.-R.; Fuks, G.; Moulin, E.; Schiffmann, O.; Dattler, D.; Funeriu, D. P.; Giuseppone, N. Dual-light control of nanomachines that integrate motor and modulator subunits. *Nat. Nanotechnol.* **2017**, *12*, 540–545.

(14) Eelkema, R.; Pollard, M. M.; Vicario, J.; Katsonis, N.; Ramon, B. S.; Bastiaansen, C. W. M.; Broer, D. J.; Feringa, B. L. Nanomotor rotates microscale objects. *Nature* **2006**, *440*, 163–163.

(15) Wang, J.; Feringa, B. L. Dynamic Control of Chiral Space in a Catalytic Asymmetric Reaction Using a Molecular Motor. *Science* **2011**, *331*, 1429–1432.

(16) Chen, K.-Y.; Ivashenko, O.; Carroll, G. T.; Robertus, J.; Kistemaker, J. C. M.; London, G.; Browne, W. R.; Rudolf, P.; Feringa, B. L. Control of Surface Wettability Using Tripodal Light-Activated Molecular Motors. *J. Am. Chem. Soc.* **2014**, *136*, 3219–3224.

(17) Feringa, B. L.; Koumura, N.; Zijlstra, R. W. J.; van Delden, R. A.; Harada, N. Light-driven monodirectional molecular rotor. *Nature* **1999**, *401*, 152–155.

(18) Koumura, N.; Geertsema, E. M.; Van Gelder, M. B.; Meetsma, A.; Feringa, B. L. Second Generation Light-Driven Molecular Motors. Unidirectional Rotation Controlled by a Single Stereogenic Center with Near-Perfect Photoequilibria and Acceleration of the Speed of Rotation by Structural Modification. *J. Am. Chem. Soc.* **2002**, *124*, 5037–5051.

(19) Kistemaker, J. C. M.; Štacko, P.; Visser, J.; Feringa, B. L. Unidirectional rotary motion in achiral molecular motors. *Nat. Chem.* **2015**, *7*, 890–896.

(20) Pollard, M. M.; Meetsma, A.; Feringa, B. L. A redesign of light-driven rotary molecular motors. *Org. Biomol. Chem.* **2008**, *6*, 507–512.

(21) Klok, M.; Boyle, N.; Pryce, M. T.; Meetsma, A.; Browne, W. R.; Feringa, B. L. MHz unidirectional rotation of molecular rotary motors. *J. Am. Chem. Soc.* **2008**, *130*, 10484–10485.

(22) Wezenberg, S. J.; Chen, K. Y.; Feringa, B. L. Visible-Light-Driven Photoisomerization and Increased Rotation Speed of a Molecular Motor Acting as a Ligand in a Ruthenium(II) Complex. *Angew. Chem., Int. Ed.* **2015**, *54*, 11457–11461.

DOI: 10.1021/jacs.9b03237
J. Am. Chem. Soc. 2019, 141, 7622–7627

(23) Faulkner, A.; van Leeuwen, T.; Feringa, B. L.; Wezenberg, S. J. Allosteric Regulation of the Rotational Speed in a Light-Driven Molecular Motor. *J. Am. Chem. Soc.* **2016**, *138*, 13597−13603.
(24) van Leeuwen, T.; Danowski, W.; Pizzolato, S. F.; Štacko, P.; Wezenberg, S. J.; Feringa, B. L. Braking of a Light-Driven Molecular Rotary Motor by Chemical Stimuli. *Chem. - Eur. J.* **2018**, *24*, 81−84.
(25) Bléger, D.; Hecht, S. Visible-Light-Activated Molecular Switches. *Angew. Chem., Int. Ed.* **2015**, *54*, 11338−11349.
(26) Cnossen, A.; Hou, L.; Pollard, M. M.; Wesenhagen, P. V.; Browne, W. R.; Feringa, B. L. Driving Unidirectional Molecular Rotary Motors with Visible Light by Intra- And Intermolecular Energy Transfer from Palladium Porphyrin. *J. Am. Chem. Soc.* **2012**, *134*, 17613−17619.
(27) van Leeuwen, T.; Pol, J.; Roke, D.; Wezenberg, S. J.; Feringa, B. L. Visible-Light Excitation of a Molecular Motor with an Extended Aromatic Core. *Org. Lett.* **2017**, *19*, 1402−1405.
(28) van Delden, R. A.; Koumura, N.; Schoevaars, A.; Meetsma, A.; Feringa, B. L. A donor−acceptor substituted molecular motor: unidirectional rotation driven by visible light. *Org. Biomol. Chem.* **2003**, *1*, 33−35.
(29) Greb, L.; Lehn, J.-M. Light-Driven Molecular Motors: Imines as Four-Step or Two-Step Unidirectional Rotors. *J. Am. Chem. Soc.* **2014**, *136*, 13114−13117.
(30) Greb, L.; Eichhöfer, A.; Lehn, J. M. Synthetic Molecular Motors: Thermal N Inversion and Directional Photoinduced C═N Bond Rotation of Camphorquinone Imines. *Angew. Chem., Int. Ed.* **2015**, *54*, 14345−14348.
(31) Guentner, M.; Schildhauer, M.; Thumser, S.; Mayer, P.; Stephenson, D.; Mayer, P. J.; Dube, H. Sunlight-powered kHz rotation of a hemithioindigo-based molecular motor. *Nat. Commun.* **2015**, *6*, 8406.
(32) Huber, L. A.; Hoffmann, K.; Thumser, S.; Böcher, N.; Mayer, P.; Dube, H. Direct Observation of Hemithioindigo-Motor Unidirectionality. *Angew. Chem., Int. Ed.* **2017**, *56*, 14536−14539.
(33) Gerwien, A.; Mayer, P.; Dube, H. Photon-Only Molecular Motor with Reverse Temperature-Dependent Efficiency. *J. Am. Chem. Soc.* **2018**, *140*, 16442−16445.
(34) Luňák, S.; Horáková, P.; Lyčka, A. Absorption and fluorescence of arylmethylidenoxindoles and isoindigo. *Dyes Pigm.* **2010**, *85*, 171−176.
(35) Cnossen, A.; Kistemaker, J. C. M.; Kojima, T.; Feringa, B. L. Structural Dynamics of Overcrowded Alkene-Based Molecular Motors during Thermal Isomerization. *J. Org. Chem.* **2014**, *79*, 927−935.
(36) Kistemaker, J. C. M.; Pizzolato, S. F.; van Leeuwen, T.; Pijper, T. C.; Feringa, B. L. Spectroscopic and Theoretical Identification of Two Thermal Isomerization Pathways for Bistable Chiral Overcrowded Alkenes. *Chem. - Eur. J.* **2016**, *22*, 13478−13487.
(37) Vicario, J.; Meetsma, A.; Feringa, B. L. Controlling the speed of rotation in molecular motors. Dramatic acceleration of the rotary motion by structural modification. *Chem. Commun.* **2005**, No. 47, 5910−5912.
(38) Dietrich, U.; Hackmann, M.; Rieger, B.; Klinga, M.; Leskelä, M. Control of Stereoerror Formation with High-Activity "Dual-Side" Zirconocene Catalysts: A Novel Strategy To Design the Properties of Thermoplastic Elastic Polypropenes. *J. Am. Chem. Soc.* **1999**, *121*, 4348−4355.
(39) In addition to the unstable *Z*-**1** isomer, the unstable *E*-**1** isomer can also be observed. This is most likely due to internal heating in the sample, causing the THI to occur. When a sample of motor **1** in THF-d_8 is irradiated at −15 °C, no further isomerization processes are observed (Figure S4).

DOI: 10.1021/jacs.9b03237
J. Am. Chem. Soc. 2019, 141, 7622−7627